Coupled-channels treatment of deformed proton emitters

Henning Esbensen and Cary N. Davids
Physics Division, Argonne National Laboratory, Argonne, Illinois 60439
(Received 30 June 2000; published 20 December 2000)

The structure of deformed proton emitters is studied in a coupled-channels treatment. The wave function of a decaying state is determined as a standing wave, i.e., for an energy that is real. The decay rate is calculated from a Green's function method, treating the influence of the long-range Coulomb multipole interactions to first order. The results are compared to predictions made in the adiabatic limit and to measurements. It is shown that the decay of the ^{131}Eu$(3/2^+)$ ground state to the ground state of ^{130}Sm is quite sensitive to deformation in the spin-orbit force. It is found that the ground state decay of ^{141}Ho$(7/2^-)$ is poorly described in the coupled-channels approach. This is ascribed to Coriolis mixing, which is too strong in the absence of pairing effects.

DOI: 10.1103/PhysRevC.63.014315 PACS number(s): 23.50.+z, 21.10.Tg, 24.10.Eq, 27.60.+j

I. INTRODUCTION

Information about the structure of deformed nuclei beyond the proton drip line has recently been obtained from measurements of the decay rate and the energy of the emitted protons. One example is the ground state decay of ^{131}Eu to the ground state [1,2] and to an excited state [2] of ^{130}Sm. Another example is the decay of ^{141}Ho, both from the ground state [1] and from an isomeric state [3], to the ground state in ^{140}Dy. The daughter nuclei are expected to fall in a region of large quadrupole deformations [4].

The measurements were analyzed in a particle-rotor model, with an unbound proton interacting with an axially symmetric, quadrupole deformed core, making use of several approximations [1,2]. Thus the wave functions of the decaying states were obtained by diagonalizing a deformed Hamiltonian in a spherical single-particle basis. Moreover, this was done in the adiabatic limit, where the excitation energies of the rotor are set to zero. However, the effect of rotational excitations of the daughter nucleus in the final state was included by using the Green's function method of Bugrov and Kadmensky [5].

Since the decay rate is extremely sensitive to the energy of the emitted proton, it is useful to study the wave function of a decaying state in a more consistent way. This can be done in the coupled-channels approach, where one can include non-zero core excitation energies. Moreover, the wave function of a decaying state is automatically generated by solving a set of coupled radial differential equations. Such studies have already been performed, both in the adiabatic limit [6–9], and also in the nonadiabatic case [10]. These calculations employed complex energies and the coupled equations were solved out to large distances, outside the range of the couplings. Such calculations are very time consuming, partly because the decay rate (related to the imaginary part of the complex energy) is extremely small, and partly because the range of the Coulomb quadrupole interaction is large.

A much faster method, which is employed in this work, is to solve the coupled equations for real energies. The decaying state is therefore a standing wave, and the decay rate is extracted by employing the Green's function method [5]. It has been shown [11] that the decay rate obtained from this method, in principle, is in exact agreement with the ''direct'' method [7], which employs complex energies and extracts the decay rate from the asymptotic amplitudes of the outgoing Coulomb waves. We show that the Green's function method can be used quite reliably to calculate the influence of the long-ranged Coulomb multipole interactions, so that the coupled equations need only to be solved out to 10–20 fm.

For a given total spin I of the decaying state, the included channels are labeled by (ljR), where (lj) specifies the single-particle orbits and R is the angular momentum of the core, i.e., daughter nucleus. This formulation is made in the laboratory frame, and we refer to it as the R representation because the Hamiltonian of the rotor is diagonal in this representation. This feature makes it easy to impose the correct asymptotic form of the radial wave functions at large distances.

An alternative representation is to use single-particle orbits in the body-fixed frame of the rotor. They are specified by quantum numbers (ljK), where K is the projection of the spin on the symmetry axis of the rotor. We refer to this as the K representation. It has the advantage that the interaction between the proton and the rotor is diagonal in K. This feature simplifies calculations in the adiabatic limit. In the nonadiabatic case, however, the Hamiltonian of the rotor is not diagonal in K due to Coriolis mixing. This makes it difficult to impose the correct asymptotic form of the radial wave functions. We shall see that the two representations are equivalent.

The coupled-channels approach is discussed in the next section. In Sec. III it is shown that the R representation and the K representation are related by a simple transformation, and the adiabatic limit is also discussed. In Sec. IV we discuss the significance of a deformed spin-orbit interaction compared to the monopole part of it. The numerical results we have obtained for ^{131}Eu and ^{141}Ho, both in the coupled-channels approach and in the adiabatic limit, are compared to measurements in Sec. V, and Sec. VI contains our conclusions.

II. COUPLED-CHANNELS APPROACH

We wish to determine the wave function of a nucleus consisting of a single proton interacting with an axially symmetric, deformed core. We include, for simplicity, only the ground state rotational band in the core nucleus and assume that the spectrum is of the form $E_R=(\hbar^2/2J_0)R(R+1)$, where $R=0,2,4,\ldots$. This problem is discussed in Appendix 5A of Ref. [12] as a coupled-channels scattering problem. Here we apply this formulation to determine bound states and narrow resonances.

The total wave function for a particular total spin (I,M) of the system has the form

$$\Psi_{IM}(\mathbf{r},\omega)=\sum_{ljR}\frac{\phi^I_{ljR}(r)}{r}|l(jR)IM\rangle, \tag{1}$$

where

$$|l(jR)IM\rangle=\sum_{mM_R}\langle jmRM_R|IM\rangle|RM_R\rangle|ljm\rangle \tag{2}$$

is the channel-spin wave function, obtained by coupling the single-particle, spin-angular wave functions $|ljm\rangle$ to the wave function $|RM_R\rangle$ of the rotor.

The total Hamiltonian of the proton-core system,

$$H=T+V(\mathbf{r},\omega)+V_{ls}(r)+H_R, \tag{3}$$

consists of the relative kinetic energy T, the Coulomb plus nuclear interaction $V(\mathbf{r},\omega)$, which depends on the position $\mathbf{r}$ of the proton and the orientation ω of the rotor, and the Hamiltonian H_R of the rotor. We also include a spin-orbit interaction but consider here, for simplicity, only the monopole part of it. The detailed parametrization of the interactions we have used is given in Appendix A, and the implementation of the full deformed spin-orbit interaction is discussed in Sec. IV.

To proceed, we first make a multipole expansion of the Coulomb plus nuclear interaction

$$V(\mathbf{r},\omega)=\sum_{\lambda}V_\lambda(r)P_\lambda[\cos(\theta')],$$

where θ' is the orientation angle of the nucleon with respect to the symmetry axis of the rotor. Inserting the wave function (1) into the Schrödinger equation, $H\Psi_{IM}=E\Psi_{IM}$, and projecting this equation with the channel-spin wave function $|l(jR)IM\rangle$, we obtain the following set of coupled differential equations for the radial wave functions:

$$(h_{lj}+E_R-E)\phi^I_{ljR}(r)=-\sum_{l'j'R'}\sum_{\lambda\neq 0}\langle l(jR)IM|P_\lambda[\cos(\theta')]\times|l'(j'R')IM\rangle V_\lambda(r)\phi^I_{l'j'R'}(r), \tag{4}$$

where h_{lj} includes the monopole pieces of the interaction

$$h_{lj}=\frac{\hbar^2}{2\mu}\left(-\frac{d^2}{dr^2}+\frac{l(l+1)}{r^2}\right)+V_0(r)+V_{ls}(r). \tag{5}$$

An expression for the matrix elements of the Legendre polynomials is given in Sec. III A.

A. Determination of resonances

The wave function of a proton resonance is sometimes calculated by using complex energies. The asymptotic boundary conditions, which determine the resonance, are outgoing Coulomb waves in all channels [7], i.e.,

$$\phi^I_{ljR}(r)=N^I_{ljR}[G_l(k_Rr)+iF_l(k_Rr)],\quad \text{for } r\to\infty. \tag{6}$$

Here $\hbar k_R=\sqrt{2\mu|E-E_R|}$ is the momentum of the emitted proton, and $F_l(k_Rr)$ and $G_l(k_Rr)$ are regular and irregular Coulomb wave functions, respectively. By calculating the outgoing flux of protons, one arrives at the following expression for the partial decay widths [7]:

$$\Gamma_{IR}=\sum_{lj}\Gamma^I_{ljR},\quad \text{where } \Gamma^I_{ljR}=\frac{\hbar^2k_R}{\mu}|N^I_{ljR}|^2. \tag{7}$$

The widths Γ_{IR} are extremely small in the cases of interest, typically of the order of 10^{-20} MeV, whereas the resonance energy $E_{\rm res}$ is of the order of 1 MeV. The small width arises from the height and the thickness of the Coulomb barrier. Consequently, the wave function of a resonance state falls off dramatically as it passes through the barrier, typically by 10 orders of magnitude as illustrated in Fig. 1 of Ref. [13]. It is very difficult to calculate the wave function accurately out to large distances, outside the range of the couplings, where the matching to Coulomb waves can safely be made. It requires that the energy of the resonance be determined with extremely high precision.

Alternative approaches to overcome this problem have been suggested. One example is to express the coupled equations in terms of the logarithmic derivative of the radial wave functions [6]. This method may have some advantages and is apparently more stable. Another possibility is to use the solutions one obtains in an interval $0<r<r_m$ and match them at $r=r_m$ to the solutions one obtains by an inward integration, from the asymptotic region to r_m. We shall not pursue this possibility here.

We have chosen a much simpler approach. We match our solutions to Coulomb waves at a relatively small distance, $r_m\approx 15$ fm, which is outside the range of nuclear couplings. In this first stage we ignore the effect of the long-ranged Coulomb couplings. We will include this effect in the calculation of the decay rate using the distorted wave Green's function method. Moreover, we adopt energies that are real, so our solutions are standing waves and we replace the boundary conditions (6) by

$$\phi^I_{ljR}(r)=N^I_{ljR}G_l(k_Rr),\quad \text{at } r=r_m, \tag{8a}$$

when $E>E_R$. If $E<E_R$, the radial wave functions are matched to the asymptotic form of bound state Coulomb wave functions, i.e., the Whittaker functions

$$\phi^I_{ljR}(r)=N^I_{ljR}W_{\eta,l+1/2}(2k_Rr), \quad \text{at } r=r_m, \tag{8b}$$

where $\eta=Z_De^2/(\hbar^2k_R/\mu)$. The numerical procedure we have used to determine the energy and the wave function of a resonance is discussed in detail in Appendix B.

This procedure needs some justification. First of all, it is not unreasonable to use a real energy and to determine the wave function of a narrow resonance as a standing wave. The boundary condition (8a) implies that the nuclear phase shift of the scattering state is 90°, which is a common definition of a narrow resonance. A simple way to extract the decay properties of a standing wave is to apply the outgoing, distorted wave Green's function method, which we now discuss.

B. Green's function method

Once a resonance solution $\Psi^{(\mathrm{res})}_{IM}$ has been determined, its decay properties can be determined by applying the distorted wave Green's function method associated with outgoing Coulomb waves [11,14]

$$\Psi^{(+)}_{IM}(\mathbf{r},\omega)=\int d\mathbf{r}'\,d\omega' G^{(+)}_{\mathrm{Coul}}(\mathbf{r},\omega;\mathbf{r}',\omega')\left[V(\mathbf{r}',\omega')+V_{ls}(r')-\frac{Z_De^2}{r'}\right]\Psi^{(\mathrm{res})}_{IM}(\mathbf{r}',\omega'). \tag{9}$$

The Green's function acts on the product of the resonance solution and the total interaction minus the point Coulomb interaction with the daughter nucleus, which determines the distorted Coulomb waves. This method is based on the exact Gell-Mann-Goldberger transformation [15], and it has previously been applied in studies of the proton and α decay of heavy nuclei [1,2,5].

The asymptotic form of the outgoing waves one obtains in the adiabatic limit is given in Eq. (8) of Ref. [11]. We can easily generalize that expression to the nonadiabatic case simply by inserting the correct momenta of the outgoing protons in the different channels, namely, $\hbar k_R=\sqrt{2\mu(E_{\mathrm{res}}-E_R)}$. Thus for $r\to\infty$ we obtain

$$\Psi^{(+)}_{IM}(\mathbf{r},\omega)=\sum_{ljR} N^{\mathrm{DW}}_{ljR}\frac{1}{r}[G_l(k_Rr)+iF_l(k_Rr)]|(ljR)IM\rangle, \tag{10}$$

where

$$N^{\mathrm{DW}}_{ljR}=-\frac{2\mu}{\hbar^2k_R}\int_0^{r_{\mathrm{int}}}dr\,rF_l(k_Rr)\langle l(jR)IM|V(\mathbf{r},\omega)+V_{ls}(r)-\frac{Z_De^2}{r}|\Psi^{(\mathrm{res})}_{IM}(\mathbf{r},\omega)\rangle. \tag{11}$$

The bracket denotes a matrix element with respect to the orientation of the proton and the deformed daughter nucleus, and also with respect to the spin of the proton. The radial integration is performed separately. Below we discuss the choice of the upper limit r_{int}.

The numerical calculation of Eq. (11) is fairly simple once a multipole expansion of the interaction has been performed,

$$V(\mathbf{r},\omega)+V_{ls}(r)-\frac{Z_De^2}{r}=\sum_\lambda \tilde{V}_\lambda(r)P_\lambda[\cos(\theta')].$$

The multipole terms (for $\lambda\neq0$) are identical to those considered in the coupled equations (4) but the monopole term includes also the monopole spin-orbit interaction minus the point-Coulomb interaction. Inserting this expansion, and also the expression (1) for the resonance wave function, into Eq. (11) we obtain

$$N^{\mathrm{DW}}_{ljR}=-\frac{2\mu}{\hbar^2k_R}\sum_\lambda\sum_{l'j'R'}\langle(ljR)IM|P_\lambda|(l'j'R')IM\rangle\times\int_0^{r_{\mathrm{int}}}dr\,F_l(k_Rr)\tilde{V}_\lambda(r)\phi^I_{l'j'R'}(r). \tag{12}$$

The outgoing waves in Eq. (10) are exactly of the form (6). The amplitudes N^{DW}_{ljR} will therefore determine the partial decay widths according to Eq. (7). We have previously demonstrated [11] that the amplitudes N^{DW}_{ljR} are identical to the amplitudes N^I_{ljR} defined in Eq. (8a). This is the result we obtain when we choose $r_{\mathrm{int}}=r_m$ as the upper integration limit. The proof was made in the adiabatic limit but it can easily be generalized to the nonadiabatic, coupled-channels case.

If we extrapolate the resonance wave function beyond r_m according to Eq. (8a) and extend the radial integration in Eq. (12) to $r_{\mathrm{int}}\gg r_m$, then the distorted wave method will also include the influence of the long-ranged Coulomb couplings to first order. The convergence of this method is illustrated in Fig. 1 for the ground-state to ground-state decay of ^{131}Eu, as function of the matching radius r_m. The parameters of the calculations are given in Sec. V, and the results illustrate the convergence of the coupled-channels results shown in Table I of that section. The dashed curve is the result we obtain when we choose $r_{\mathrm{int}}=r_m$. This result is identical, within the numerical accuracy, to the result of the direct method (shown by open circles), where we insert the amplitudes N^I_{ljR} from Eq. (8a) into Eq. (7). The solid curve is the result of the distorted wave method obtained by extending the integration out to $r_{\mathrm{int}}=100$ fm. It is seen to converge at a much smaller value of r_m. We find that it is sufficient to choose $r_m=15$ fm and $r_{\mathrm{int}}=100$ fm, which are the values we will employ in the following.

III. THE *K* REPRESENTATION

The particle-rotor model is usually formulated in the K representation, where K is the projection of the total spin I on the symmetry axis of the rotor. This representation is particu-

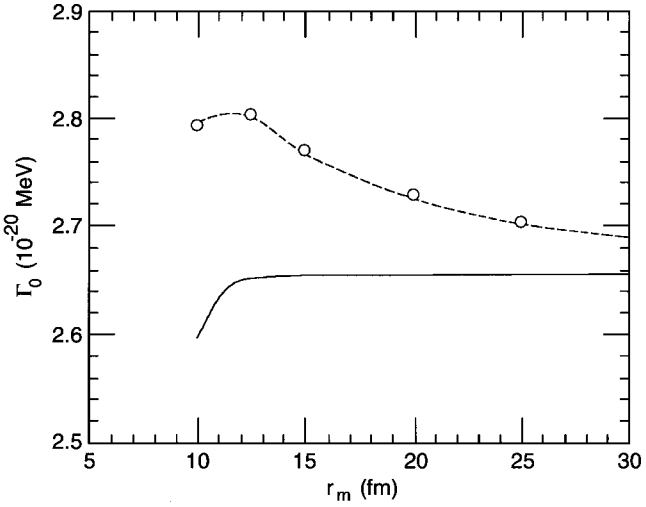

FIG. 1. Calculated ground-state–to–ground-state proton decay width for ^{131}Eu. The results are shown as functions of the matching radius r_m used in the coupled-channels calculations. The open circles are the results obtained from the direct method discussed in the text. The dashed curve is the result of the distorted wave method, Eq. (12), for $r_{\rm int}=r_m$. The solid curve is the distorted wave result obtained by extending the radial integration out to $r_{\rm int}=100$ fm.

larly convenient in the adiabatic limit and it also provides a useful way to interpret the results of a coupled-channels calculation in terms of Coriolis mixing. The K representation can be derived by expressing the single-particle states as $|ljm\rangle=\Sigma_K D^j_{mK}(\omega)|ljK\rangle_0$, in terms of the states $|ljK\rangle_0$ in the body-fixed frame of the rotor. Inserting this expression into Eq. (2), together with the wave functions for the ground state rotational band of the rotor, $\langle\omega|RM_R\rangle=\sqrt{(2R+1)/8\pi^2}D^R_{M_R0}(\omega)$, one can derive the following expression:

$$|l(jR)IM\rangle=\sum_{K>0}A^{IK}_{jR}|ljK,IM\rangle, \tag{13}$$

where

$$|ljK,IM\rangle=\sqrt{\frac{2I+1}{16\pi^2}}[D^I_{MK}(\omega)|ljK\rangle_0 + (-1)^{j-I}D^I_{M-K}(\omega)|lj-K\rangle_0], \tag{14}$$

and

$$A^{IK}_{jR}=\sqrt{\frac{2R+1}{2I+1}}\langle jKR0|IK\rangle\sqrt{1+(-1)^R}. \tag{15}$$

The derivation makes use of the sum rule, Eq. (1A-43) of Ref. [16]. It has here been assumed that R is even, as it is for the ground state rotational band of a quadrupole deformed nucleus. This feature has been built into the amplitudes (15) so that they vanish when R is odd. It is also noted that the sum in Eq. (13) is restricted to positive values of K because of a degeneracy with respect to the sign of K. Negative values of K do appear in in Eq. (14), namely, in the second term, which is the time-reversed form of the first term.

Inserting Eq. (13) into Eq. (1), we can now express the total wave function in terms of the new basis (14):

$$\Psi_{IM}(\mathbf{r},\omega)=\sum_{lj}\sum_{K>0}\frac{\phi^{IK}_{lj}(r)}{r}|ljK,IM\rangle, \tag{16}$$

where the radial wave functions are

$$\phi^{IK}_{lj}(r)=\sum_R A^{IK}_{jR}\phi^I_{ljR}(r). \tag{17}$$

It can be shown that the amplitudes (15) form an orthonormal transformation between the K and the R representation, i.e.,

$$\sum_{K>0}A^{IK}_{jR}A^{IK}_{jR'}=\delta_{R,R'}, \quad \sum_R A^{IK}_{jR}A^{IK'}_{jR}=\delta_{K,K'}. \tag{18}$$

This property makes it easy to translate the results obtained in one representation into the other. Thus we can invert Eq. (17) and obtain

$$\phi^I_{ljR}(r)=\sum_{K>0}A^{IK}_{jR}\phi^{IK}_{lj}(r). \tag{19}$$

TABLE I. Proton decay widths (in units of 10^{-20} MeV) of the ^{131}Eu($3/2^+$) ground state decay to the 0^+, 2^+, and 4^+ states of ^{130}Sm, and the branching ratio to the 2^+ state. The widths have been calculated in the adiabatic limit (adiab.) and in the coupled-channels approach (coup. chan.), both supplemented with the distorted wave Green's function technique as explained in the text. The wave number of the distorted waves was generated from the 2^+ excitation energy given in the second column. The energy of the resonance was adjusted to 950.5 keV, consistent with the measured proton energy of 932 ± 7 keV [2] corrected for recoil and electronic screening effects. The experimental results are given in the last line.

Method	E_{2^+} (keV)	Γ_0	Γ_2	Γ_4	$\Gamma_2/\Gamma_{\rm tot}$
Adiab.	0	2.88	80.3	12.9	
Adiab.	122	2.88	0.929	2.12×10^{-8}	0.244
Coup. chan.	122	2.66	0.907	2.46×10^{-8}	0.255
Experiment [2]	122	1.71 ± 0.24	0.54 ± 0.13		0.24 ± 0.05

A. Coupled equations in the *K* representation

The matrix elements of the Legendre polynomials are particularly simple in the *K* representation, Eq. (14). The integration over the orientation ω of the core is trivial because it only involves the orthogonal *D* functions. The single-particle matrix elements are evaluated in the body-fixed rest frame of the rotor. They are diagonal in *K* and have the explicit form [see Eq. (3A-14) of Ref. [16]]

$$\langle ljK|P_\lambda[\cos(\theta')]|l'j'K\rangle_0 = (-1)^\lambda \langle j'K\lambda 0|jK\rangle \langle j\tfrac{1}{2}\lambda 0|j'\tfrac{1}{2}\rangle, \tag{20}$$

when $l'+\lambda-l$ is even, and zero when $l'+\lambda-l$ is odd. Thus when the λ's are even numbers, which is the case for a quadrupole deformed core, we see that the even and the odd parity single-particle states are completely decoupled.

Let us also express the couplings in the *R* representation that appear in Eq. (4), in terms of the single-particle matrix elements (20). Thus, if we insert the expression (13) for the spin-angular wave functions in the *R* representation, we obtain

$$\langle l(jR)IM|P_\lambda[\cos(\theta')]|l'(j'R')IM\rangle = \sum_{K>0} A^{IK}_{jR}\langle ljK|P_\lambda[\cos(\theta')]|l'j'K\rangle_0 A^{IK}_{j'R'}. \tag{21}$$

The coupled equations in the *K* representation can be obtained by multiplying Eq. (4) by A^{IK}_{jR}, and next summing over *R*. In this procedure, we can make use of Eq. (17), and the sum rules (18) when dealing with the coupling matrix elements (21). The only problem is caused by the rotational energy E_R of the core. However, this term can be dealt with by inserting the expression (19) for the radial wave functions. Thus we obtain

$$[h_{lj}-E]\phi^{IK}_{lj} + \sum_{K'>0} W^{jI}_{KK'}\phi^{IK'}_{lj} = -\sum_{l'j'}\sum_{\lambda>0}\langle ljK|P_\lambda|l'j'K\rangle_0 V_\lambda(r)\phi^{IK}_{l'j'}, \tag{22}$$

where

$$W^{jI}_{KK'} = \sum_R A^{IK}_{jR} E_R A^{IK'}_{jR}. \tag{23}$$

The coupling matrix (23) has diagonal as well as off-diagonal terms, which are independent of the radial coordinate *r*. The off-diagonal terms cause some difficulties when imposing the asymptotic behavior of the radial wave functions, $\phi^{IK}_{lj}(r)$, for $r\to\infty$, in contrast to the simple form Eq. (8) in the *R* representation.

One can derive explicit expressions for the rotational couplings if one assumes a constant moment of inertia, i.e., $E_R = (\hbar^2/2J_0)R(R+1)$. The diagonal part of the coupling is then (see Eqs. (4A-9),(4A-10) of Ref. [12])

$$W^{jI}_{KK} = \frac{\hbar^2}{2J_0}[I(I+1)+j(j+1)-2K^2 + \delta_{K,1/2}(-1)^{I+j}(I+1/2)(j+1/2)]. \tag{24}$$

The off-diagonal coupling is caused by the Coriolis force which acts between neighboring *K* values, $K'=K\pm 1$. For a constant moment of inertia one obtains (see Ref. [17])

$$W^{jI}_{K,K+1} = W^{jI}_{K+1,K} = -\frac{\hbar^2}{2J_0}\sqrt{(I-K)(I+K+1)(j-K)(j+K+1)}. \tag{25}$$

These are the couplings that effectively enter into the coupled-channels calculations performed in the *R* representation. We note that rotational spectra are usually analyzed in the *K* representation, and that it is necessary to reduce the strength of the Coriolis coupling, in order to reproduce observed spectra. The necessary reduction may be explained by the pairing and two-body recoil effects discussed in Ref. [18]. We shall not consider such effects here. Instead, we perform our calculations in the *R* representation as described in Sec. II. Discrepancies with measurements may then indicate the need for improvements.

B. Adiabatic limit

The *K* representation is very convenient in the adiabatic limit, where the rotational energy of the core is set to zero and the coupled equations (22) become diagonal in *K*. The number of coupled channels is therefore much smaller for large values of *K*. It is identical to the number of single-particle orbits that one includes, with the restriction that $j \geqslant K$. The adiabatic limit provides useful guidance for locating the band heads of the different rotational bands one obtains in the coupled-channels approach.

As mentioned earlier, one can repair some of the shortcomings of the adiabatic approximation when calculating the partial decay widths to excited states of the daughter nucleus by using the distorted wave Green's function method. Thus, if we have obtained the radial wave functions $\phi^{IK}_{l'j'}$ for a given *K* in the adiabatic limit, we can construct the associated radial wave functions in the *R* representation $\phi^{I}_{l'j'R'} = A^{IK}_{j'R'}\phi^{IK}_{l'j'}$, according to Eq. (19). Inserting these wave functions into Eq. (12), and also the expression (21) for the matrix elements of the Legendre polynomials, one can use the second sum rule in Eq. (18) to perform the summation over R'. The final expression is

$$N^{\mathrm{DW}}_{ljR} = -\frac{2\mu}{\hbar^2 k_R} A^{IK}_{jR}\sum_{\lambda l'j'}\langle ljK|P_\lambda|l'j'K\rangle \times \int_0^{r_{\mathrm{int}}} dr F_l(k_R r)\tilde{V}_\lambda(r)\phi^{IK}_{l'j'}(r). \tag{26}$$

This expression is consistent with Eq. (17) in Ref. [11] for the ground-state–to–ground-state decay. The decay rate to

an excited state of the daughter nucleus, however, is considerably reduced when the correct asymptotic momentum $\hbar k_R$ is employed in the radial matrix element of Eq. (26). This is illustrated in Table I of Sec. V.

IV. DEFORMED SPIN-ORBIT INTERACTION

We have so far considered only the monopole part of the spin-orbit interaction. Using this approximation, we have not been able to reproduce recent calculations of the ground state decay of ^{131}Eu by Maglione and Ferreira [9]. They included all multipole components and performed their calculations in the adiabatic limit. We therefore decided to go beyond the monopole approximation.

The deformed spin-orbit interaction is often written as [19]

$$V_{ls}(r,\theta)=4V_{so}([\nabla f(r,\theta)]\times\mathbf{p})\cdot\mathbf{s}, \tag{27}$$

where θ is the angle between $\mathbf{r}$ and the symmetry axis of the axially symmetric rotor, and $f(r,\theta)$ is the deformed Fermi function used in Appendix A. This form was applied by Sherif [19] to analyze proton scattering data but his expressions are not so easy to use in our case. We have therefore in Appendix C [Eqs. (C3),(C8a)–(C8b)], derived the following expression:

$$V_{ls}(r,\theta)=4V_{so}\sum_{\lambda}\left(\frac{1}{r}\frac{df_\lambda}{dr}P_\lambda\mathbf{l}\cdot\mathbf{s}-\frac{f_\lambda}{r}[\mathbf{l}\cdot\mathbf{s},P_\lambda]\frac{d}{dr}\right.$$
$$\left.-\frac{f_\lambda}{r^2}\frac{dP_\lambda}{d\cos(\theta)}\frac{\mathbf{r}\cdot\mathbf{s}}{r}l_z\right), \tag{28}$$

where we have used the multipole expansion $f(r,\theta)=\Sigma_\lambda f_\lambda(r)P_\lambda[\cos(\theta)]$. The spin-angular matrix elements of this interaction are given in Eqs. (C9)–(C11) in the intrinsic system of the rotor, and one can directly include these couplings in the adiabatic limit. One can also transform the couplings into the R representation, according to Eq. (21), and include them in the coupled equations (4).

To illustrate the significance of including the full deformed spin-orbit interaction we show in Fig. 2 the branching ratio $\Gamma_2/\Gamma_{\rm tot}$ for the ^{131}Eu$(3/2^+)$ ground state decay to the 2^+ excited state of the daughter nucleus. The calculations were performed in the adiabatic limit using the parametrization discussed in Appendix A, and the results are shown as functions of the spin-orbit strength. The solid curves are the results we obtain with the monopole ($\lambda=0$) and the full deformed spin-orbit interaction (all λ's). Both calculations employed the orientation-dependent diffuseness defined in Eq. (A6). The dashed curves were obtained by ignoring the θ dependence of the diffuseness. This correction has evidently a very small effect in this case. The two horizontal dashed lines show the error band of the measurement [2].

The monopole spin-orbit force reproduces the measurement at a strength of about 6 MeV fm^2. The open circle is the adiabatic result of Ref. [10], which employed the Chepurnov parameters and included only the monopole part of the spin-orbit force. It is consistent with our ($\lambda=0$) result. The full deformed spin-orbit interaction produces a smaller branching ratio and fits the measurement at $V_{so}\approx 10$ MeV fm^2. This value is close to the spin-orbit strength of the ''universal'' interaction that was employed in Ref. [9]. The result obtained there is shown by the diamond, and it is consistent with our (all λ's) calculation.

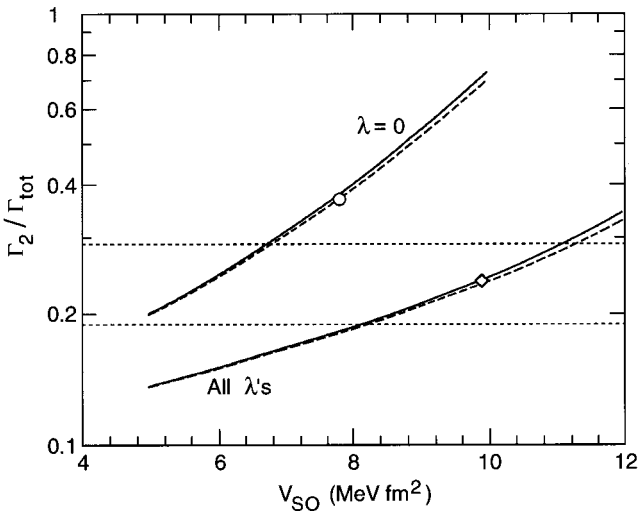

FIG. 2. Branching ratio for the ^{131}Eu ground state decay to the first 2^+ excited state of ^{130}Sm, calculated in the adiabatic limit as a function of the spin-orbit strength. The two sets of calculations were based on the monopole ($\lambda=0$) and the full deformed spin-orbit interaction (all λ's), respectively. The solid curves represent results with the orientation-dependent diffuseness, Eq. (A6), while the dashed curves ignore this dependence. The open circle is the adiabatic ($\lambda=0$) result of Ref. [10], and the diamond is the (all λ's) result of Ref. [9]. The horizontal dashed lines represent the experimental error band [2].

The total proton decay width we obtain is shown in Fig. 3. The two horizontal dashed lines are again the error band of the measurement [2]. The decay width obtained in Ref. [9],

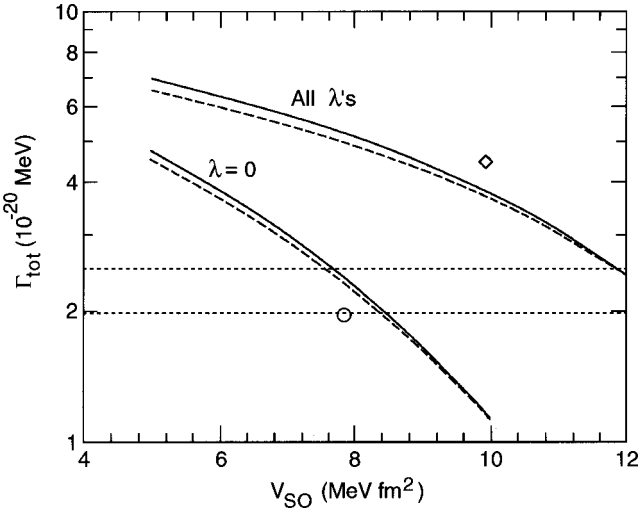

FIG. 3. Calculated total proton decay width for ^{131}Eu. The symbols are the same as in Fig. 2, except the open circle which is the coupled-channels result of Ref. [10] obtained with a monopole spin-orbit force.

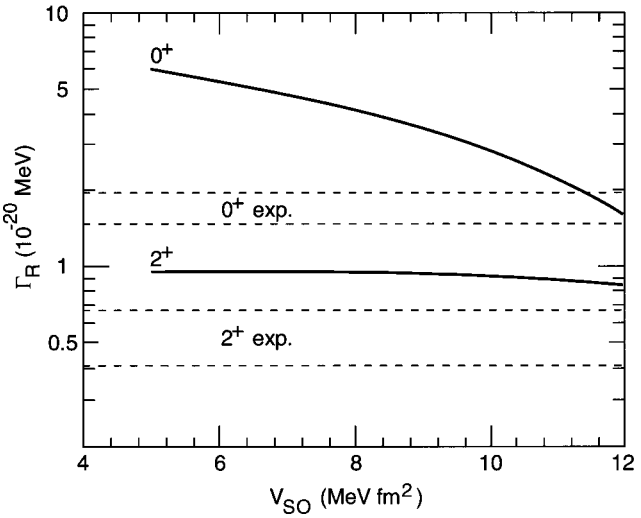

FIG. 4. Calculated widths for the ground state proton decay of ^{131}Eu to the 0^+ ground state and 2^+ excited state of ^{130}Sm as functions of the spin-orbit strength. The calculations employed the full deformed spin-orbit interaction. The horizontal dashed lines represent the experimental error bands [2].

shown by the diamond, is slightly larger than our result (all λ's). This is mainly caused by a slightly larger radius of the nuclear potential, increasing r_0 from 1.25 to 1.275 fm, whereas the branching ratio is insensitive to this variation. The open circle is the result of the coupled-channels calculations performed in Ref. [10]. It is smaller than our adiabatic calculation ($\lambda=0$). We have therefore performed a coupled-channels calculation, with the same interaction and deformation as used in Ref. [10]. Thus we obtain a total proton decay width of 2.00×10^{-20} MeV and a 2^+ branching ratio of 0.40, in very good agreement with the decay width of 1.98×10^{-20} MeV (based on the quoted 23 ms half-life) and branching ratio of 0.39 obtained in Ref. [10].

The present work shows that the branching ratio for the decay of the ^{131}Eu($3/2^+$) ground state is a very sensitive probe of the spin-orbit force. The reason is that the decay to the 0^+ ground state of ^{130}Sm originates from a very small component of the ground state wave function, with a $d_{3/2}$ wave coupled to the 0^+ state of the core. The dominant component is a $d_{5/2}$ wave coupled to the 2^+ state of the core. Thus, if we change the strength of the spin-orbit interaction, the relative weights of the $d_{3/2}$ and $d_{5/2}$ components will change. The resulting decay widths we obtain with the full deformed spin-orbit interaction is illustrated in Fig. 4. It is seen that the decay width to the 0^+ state is quite sensitive to the spin-orbit strength, whereas the 2^+ decay width is essentially independent of it.

We conclude that it is important to use the full deformed spin-orbit interaction in an analysis of the ^{131}Eu($3/2^+$) decay. We are then able to reproduce the measured branching ratio (in the adiabatic limit) for the spin-orbit strength $V_{so}\approx10$ MeV fm^2, which is consistent with the values commonly used in structure calculations of heavy nuclei [20,21]. Moreover, we are able to reproduce the results of Refs. [9,10] with our numerical methods. This gives us confidence in our approach of supplementing the structure calculation with the distorted wave Green's function method.

V. APPLICATIONS TO DEFORMED PROTON EMITTERS

In this section we apply the coupled-channels approach, and also the adiabatic limit, to study the proton decay of ^{131}Eu and ^{141}Ho. We include all single-particle orbits with $l\leqslant7$, and all the necessary states of the ground state rotational band of the daughter nucleus. We also include all multipole components of the Coulomb, nuclear, and the full deformed spin-orbit interactions, i.e., up to $\lambda=14$ for $l_{\max}=7$, and we employ the angle-dependent diffuseness defined in Eq. (A6).

There are several adjustable parameters in our particle-rotor model. We have chosen the radius parameter $r_0=1.25$ fm and diffuseness $a=0.65$ fm for the nuclear and spin-orbit interactions, as discussed in Appendix A. The parameters of the charge distribution of the core are also kept fixed, with $r_0=1.22$ fm and $a_C=0.56$ fm. Guided by the results we obtained in the previous section we choose the strength $V_{so}=10$ MeV fm^2 of the deformed spin-orbit interaction. The depth of the nuclear potential, typically of the order of 50 to 55 MeV, is adjusted so that the measured energy of the decaying state is reproduced.

Previous analyses have focused on the sensitivity to the quadrupole deformation parameter β_2 but we adopt the predicted value [4] of $\beta_2=0.33$ for ^{130}Sm. For ^{140}Dy we use $\beta_2=0.267$ and include also the predicted $\beta_4=-0.05$. The rotational spectrum of the daughter nucleus $E_R=(\hbar^2/2J_0)R(R+1)$, is generated from the measured 2^+ excitation energy of 122 keV for ^{130}Sm [2], and an estimated value of 160 keV for ^{140}Dy [22].

We have already applied the above parameters for ^{131}Eu in Figs. 1–4. In Fig. 1 we illustrated the rapid convergence of the distorted wave Green's function method as a function of the matching radius. Based on that result, we shall always use the matching radius $r_m=15$ fm, and the upper limit $r_{\rm int}=100$ fm for the radial integration which determines the distorted wave amplitudes, Eqs. (12) and (26).

The calculated decay rate to the ground state of the daughter nucleus is extremely sensitive to the energy and the angular momentum of the emitted proton. It is therefore fairly easy, in most cases, to determine the spin of the decaying state. Previous analyses [2,9,10] have shown that the ground state of ^{131}Eu is a $3/2^+$ state, and the ground state of ^{141}Ho is a $7/2^-$ state. Our analysis confirms this determination, and we shall therefore not discuss other candidates.

A. Proton decay of ^{131}Eu

The single-particle spectrum we obtain in the adiabatic limit for ^{131}Eu is shown in Fig. 5 as function of the quadrupole deformation parameter β_2. The solid curves are the energies of positive parity states, whereas the dashed curves are the energies of the negative-parity states. The depth of the deformed Woods-Saxon well, $V_N^{(0)}=-52.784$ MeV, was adjusted at the predicted deformation, $\beta_2=0.33$, to produce a $3/2^+$ ground state energy of 950.5 keV. This energy is con-

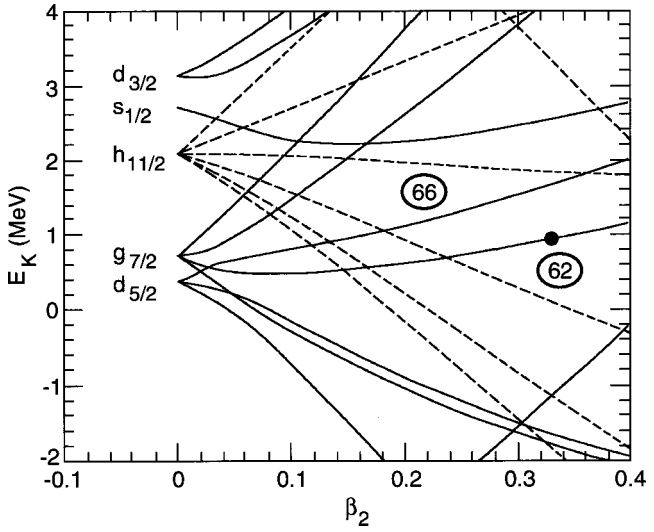

FIG. 5. Single-particle energy spectrum obtained in the adiabatic limit for ^{131}Eu as a function of the quadrupole deformation β_2. The depth of the deformed Woods-Saxon well was adjusted to produce a $3/2^+$ ground state energy of 950.5 keV at $\beta_2=0.33$, which is indicated by the filled circle.

sistent with the measured energy of the emitted protons [2] when corrected for recoil and electronic screening effects. The $3/2^+$ ground state is shown by the solid point. It originates from the $g_{7/2}$ state in the spherical limit, and it is often referred to as the $[422]3/2^+$ Nilsson orbit. Counting the levels from below it is seen that this state is indeed at the Fermi surface for $Z=63$.

The spectrum shown in Fig. 5 is similar to that obtained in Ref. [9]. There are minor differences, due to the slightly larger nuclear radius used there as mentioned in Sec. IV, where we compared the calculated branching ratio and total decay width. The $3/2^+$ ground state predicted in Ref. [10], based on a monopole spin-orbit force, was the $[411]3/2^+$ Nilsson orbit, which originates from the $d_{5/2}$ state in the spherical limit. This is a minor detail, which is related to the ordering of the $d_{5/2}$ and the $g_{7/2}$ levels in the spherical limit. Thus the calculated decay widths shown in Fig. 3 are associated with the $[411]3/2^+$ Nilsson orbit at small values of V_{so}, and with the $[422]3/2^+$ orbit at large values of V_{so}.

The decay rates we obtain in the adiabatic limit and in the coupled-channels approach, both supplemented with the Green's function method to estimate the influence of the long-ranged Coulomb multipole couplings [see Eqs. (12) and (26)], are shown in Table I. The first line gives the partial decay widths we obtain when we set the excitation energies of the final states of the daughter nucleus equal to zero in the Green's function method. The second line shows the results we obtain when we use the correct final state energies. The resulting decay widths to the 2^+ and 4^+ states are reduced considerably compared to the first line, but they agree quite well with the results we obtain in the coupled-channels approach, which are shown in the third line. Moreover, the predicted branching ratio for the 2^+ final state is in very good agreement with the coupled-channels result and with the measurement. The calculated decay widths are larger than the measured values, indicating a spectroscopic factor of the order of 0.6.

TABLE II. Resonance energies and proton decay widths (in units of 10^{-20} MeV) for the ground state rotational band of ^{131}Eu, calculated in the coupled-channels approach. Also shown is the calculated branching ratio to the 2^+ state, and the half-life.

I^π	E_I (keV)	Γ_0	Γ_2	Γ_4	Γ_2/Γ_{tot}	$t_{1/2}$ (μs)
$3/2^+$	950.5	2.66	0.907	2.46×10^{-8}	0.255	12800
$5/2^+$	1052.2	625.0	4.24	9.17×10^{-5}	0.0067	72.5
$7/2^+$	1194.5	10.3	1366.0	0.0825	0.9925	33.0
$9/2^+$	1377.7	5.51	91840.0	28.5	0.9996	0.5

It is remarkable that the Green's function method is able to repair the shortcomings of the adiabatic approximation and reproduce the coupled-channels results so well. We shall see that this feature is true only when Coriolis mixing is weak, as it is for low spin states. Thus the $K=3/2$ component makes up 99.8% of the ground state wave function in the coupled-channels calculation.

The coupled-channels approach makes it possible to calculate the rotational spectrum build on the ^{131}Eu$(3/2^+)$ ground state. The results are shown in Table II. The moment of inertia extracted from the calculated spectrum is almost identical to the moment of inertia of the daughter nucleus. The decay widths to the 4^+ state (and also to higher spin states) are small and can be ignored. The proton decay pattern is qualitatively the same as predicted by the monopole spin-orbit force in Ref. [10]. The main difference is in the decay width of the ground state; it is 80% larger in our calculation, which employs the full deformed spin-orbit interaction.

B. Proton decay of ^{141}Ho

From the single-particle spectrum shown in Fig. 5 one would expect that the ground state spin of ^{141}Ho, with Z=67, is $7/2^-$ since the predicted quadrupole deformation of the daughter is $\beta_2=0.267$. This is indeed the result we obtain when we carry out the detailed calculation, in agreement with the findings of previous analyses [1,7,10]. From these systematics we expect the ground state spin of ^{A}Tb, with $Z=65$ and $A\approx135$, to be $5/2^+$ since the predicted quadrupole deformation of the associated Gd isotopes [4] is $\beta_2\approx0.3$.

The decay widths we obtain for the $7/2^-$ ground state are shown in the first part of Table III. The decay rate to the ground state of ^{140}Dy that we obtain in the adiabatic limit is almost a factor of 5 larger than the result of the coupled-channels approach. While the adiabatic result seems reasonable in comparison to the measurement, with a spectroscopic factor of 0.66, the coupled-channels result is unrealistic, yielding a spectroscopic factor of 3.2. Moreover, the branching ratio to the 2^+ state, predicted by the coupled-channels calculation, is much higher than the upper limit of 1% set by experiments [23]. These discrepancies lead us to believe that the coupled-channels approach is unreliable in this case.

The large discrepancy between the adiabatic and the coupled-channels result is caused by strong Coriolis mixing

TABLE III. Proton decay widths (in units of 10^{-20} MeV), branching ratio to the 2^+ state, and the total proton decay half-life of the $7/2^-$ ground state at 1.190 MeV, and the $1/2^+$ isomeric state at 1.256 MeV in ^{141}Ho. The results obtained in the adiabatic (adiab.) and the coupled-channels approach (coup. chan.) are compared to measurements. The adopted 2^+ excitation energy of ^{140}Dy is 160 keV.

Method	I^π	Γ_0	Γ_2	Γ_2/Γ_{tot}	$t_{1/2}$
Adiab.	$7/2^-$	16.5	0.45	0.027	2.7 ms
Coup. chan.	$7/2^-$	3.38	0.27	0.079	12.5 ms
Experiment [1,23]	$7/2^-$	10.9 ± 1.0		<0.01	4.2 ± 0.4 ms
Adiab.	$1/2^+$	21700	330	0.015	2.1 μs
Coup. chan.	$1/2^+$	22530	317	0.014	2.0 μs
Experiment [3]	$1/2^+$	5700 ± 2140			8 ± 3 μs
Experiment [23]	$1/2^+$	7020 ± 1080		<0.01	6.5 ± 1 μs

in the latter. In fact, only 80% of the $7/2^-$ ground state wave function belongs to the $K=7/2$ band. In a more realistic calculation, which would include pairing effects, Coriolis mixing would be quenched. We therefore suspect that the adiabatic limit gives a more realistic estimate. We note that the coupled-channels calculation of Ref. [10], based on a monopole spin-orbit force, also predicted a small width of 2.8×10^{-20} MeV.

The decay rates we obtain for the $1/2^+$ isomeric state in ^{141}Ho are given in the second part of Table III. Here the adiabatic limit and the coupled-channels approach give almost the same results, as we would expect for a low-spin state. They are about a factor of 3 larger than the measurement, indicating a spectroscopic factor of about 0.3. The coupled-channels results of Kruppa *et al.* [10], and also the adiabatic results of Ref. [8], are quite similar to our results. The low spectroscopic factor may indicate that the shape of the core for the $1/2^+$ state is different from the shape of the daughter nucleus, resulting in a poor overlap.

In Table IV we show the calculated rotational band build on the $1/2^+$ state. We see that the preferred proton decay branch changes from the 0^+ to the 2^+ final state at spin $5/2^+$. We also see a strong signature splitting of the rotational band, so that the $1/2^+$ and $3/2^+$ states, and also the $5/2^+$ and $7/2^+$ states, are almost degenerate.

TABLE IV. Calculated energies and proton decay widths (in units of 10^{-15} MeV) of the rotational states build on the $1/2^+$ isomer in ^{141}Ho. Also shown is the branching ratio to the 2^+ final state and the half-life. The 2^+ excitation energy of ^{140}Dy was set to 160 keV.

I^π	E_I (keV)	Γ_0	Γ_2	Γ_2/Γ_{tot}	$t_{1/2}$ (μs)
$1/2^+$	1256.0	0.225	0.0032	0.014	2.0
$3/2^+$	1268.6	0.102	0.0054	0.050	4.2
$5/2^+$	1512.1	2.65	2.57	0.492	0.087
$7/2^+$	1542.3	0.0057	1.60	0.996	0.284
$9/2^+$	1990.0	0.06	354.0	1.000	0.0013

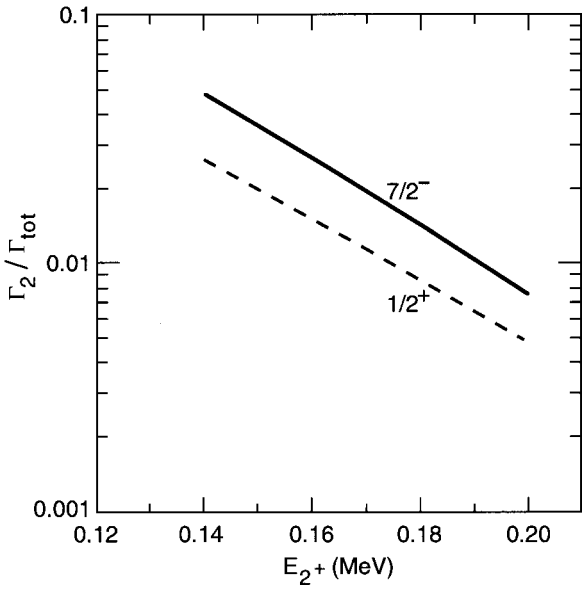

FIG. 6. Branching ratios for the proton decay of the $7/2^-$ and $1/2^+$ states in ^{141}Ho to the first 2^+ excited state in ^{140}Dy, calculated in the adiabatic limit as functions of the (unknown) excitation energy of the 2^+ final state.

There are a number of uncertainties in our calculations. In particular, the 2^+ excitation energy in the daughter nucleus ^{140}Dy is not known. This quantity strongly affects the predicted branching ratio of the proton decay. We show in Fig. 6 the predicted 2^+ branching ratio for the two proton-emitting states in ^{141}Ho, calculated in the adiabatic limit as functions of the 2^+ excitation energy in ^{140}Dy. The experimental upper limit for this quantity is 1% in both cases [23]. This suggests that the postulated value of 160 keV may be too low.

VI. CONCLUSIONS

We have investigated the proton decay of heavy, deformed nuclei in a coupled-channels description. We find that the *R* representation, which is formulated in the laboratory frame, is particularly convenient when imposing the asymptotic form of resonance wave functions. The *K* representation, which is commonly used in structure calculations, makes use of single-particle states that are expressed in the body-fixed frame of the rotor. This representation is less convenient because the Coriolis interaction is nondiagonal. It is, however, very attractive in the adiabatic limit, where the Coriolis force vanishes and the Hamiltonian becomes diagonal in the *K* quantum number, resulting in a reduction in the number of coupled channels to be considered.

We find that it is sufficient to employ real energy eigenvalues in the coupled equations, instead of dealing with complex energies with an imaginary component that is related to an extremely small decay width. The decay width can be extracted from the distorted wave Green's function technique. Moreover, it is sufficient to solve the coupled equations out to about 15 fm because the Green's function technique can be used to calculate quite reliably the influence of

the long-ranged Coulomb multipole fields. These two simplifications reduce the necessary computing time considerably.

The Green's function technique can also be applied to calculate the decay rate in the adiabatic limit, because one can implement the correct asymptotic momentum in the distorted Coulomb waves of the Green's function. This is important when one considers the decay to an excited state of the daughter nucleus. When the spin of the decaying state is low, so that Coriolis mixing is weak, we find that the partial decay widths obtained in this way are in good agreement with a nonadiabatic, coupled-channels calculation. We illustrated this point for the decay of the ^{131}Eu($3/2^+$) ground state and the $1/2^+$ isomeric state in ^{141}Ho.

The decay width of the ^{141}Ho($7/2^-$) ground state, on the other hand, is a factor of 3 smaller in the full coupled-channels approach than in the adiabatic limit. This discrepancy is caused by Coriolis mixing, which is particularly strong for a high-spin state. The effect of pairing could possibly play an important role and lead to a reduction of the Coriolis mixing. Since we have not considered this effect explicitly, we expect that the adiabatic approximation, supplemented with the distorted wave Green's method, gives a more realistic estimate of the decay width, in particular for a state with high spin.

When dealing with the decay from a small component of a resonance wave function, we find that it is necessary to consider the full deformed spin-orbit interaction, instead of just the monopole term. An example is the decay of the ^{131}Eu($3/2^+$) ground state to the 0^+ ground state of ^{130}Sm. The associated component of the ground state wave function is small and its magnitude is very sensitive to the spin-orbit interaction. The decay to the 2^+ state of ^{130}Sm, on the other hand, involves a much larger fraction of the ground state wave function and it is essentially insensitive to the spin-orbit force. Using a deformed spin-orbit interaction, with a strength that is commonly used in structure calculations, we are able to reproduce the measured branching ratio to the two states. Moreover, the measured proton decay width is about 60% of the calculated width.

The most needed improvement in the nonadiabatic, coupled-channels approach is to consider the effect of pairing, not only in terms of a spectroscopic factor, but more importantly, to implement the quenching of the Coriolis mixing that it may cause. It may also be necessary to go beyond the particle-rotor model and consider a nonperfect overlap of the core and the daughter nucleus, in order to explain the measured decay width of the ^{141}Ho($1/2^+$) isomeric state, which is a factor of 3 smaller than our prediction.

ACKNOWLEDGMENTS

This work was supported by the U.S. Department of Energy, Nuclear Physics Division, under Contract No. W-31-109-ENG-38.

APPENDIX A: PARAMETRIZATION OF INTERACTIONS

The nuclear interaction between the valence proton and the deformed core nucleus is parametrized in terms of the Fermi function $f(x)=[1+\exp(x)]^{-1}$ as

$$V_N(r,\theta)=V_N^{(0)}f\left(\frac{r-R(\theta)}{a}\right),$$

where

$$R(\theta)=R_N\left[1+\sum_\lambda \beta_\lambda Y_{\lambda 0}(\theta)\right], \tag{A1}$$

and θ is the angle between $\mathbf{r}$ and the symmetry axis of the core. The radius is calculated as

$$R_N=r_0\left(\frac{A_D}{C(\beta_2)}\right)^{1/3},$$

where

$$C(\beta_2)=\int\frac{d\Omega}{4\pi}\left(1+\sum_\lambda \beta_\lambda Y_{\lambda 0}(\theta)\right)^3 \tag{A2}$$

is a volume preserving factor, and A_D is the mass number of the core. We have used $\beta_2=0.33$ for ^{131}Eu, and $\beta_2=0.267$ and $\beta_4=-0.05$ for ^{141}Ho, which are the predicted deformations [4] of the daughter nuclei ^{130}Sm and ^{140}Dy, respectively.

We consider here, for simplicity, only the monopole component of the spin-orbit interaction. It is parametrized as

$$V_{ls}(r)=4V_{so}\frac{1}{r}\frac{d}{dr}f_0(r)\mathbf{l}\cdot\mathbf{s}, \tag{A3}$$

where $f_0(r)$ is the monopole term of the deformed Fermi function that appears in Eq. (A1). We discuss in Sec. IV how to implement higher multipole components of a deformed spin-orbit interaction. The parameters to determine so far are r_0, a, V_{so}, and $V_N^{(0)}$.

For scattering states [24,25], the empirical radius parameter r_0 falls in the range from 1.17 to 1.25 fm, and the spin-orbit strength is $V_{so}\approx 6$ MeV fm^2. In structure calculations [20,21], one usually uses larger radii, with $r_0\approx 1.24$ to 1.275 fm, and a much stronger spin-orbit strength, $V_{so}\approx 9-10$ MeV fm^2. We have chosen the compromise $r_0=1.25$ fm and used $a=0.65$ fm in all of our calculations. The spin-orbit strength is discussed in Sec. IV, where we find that $V_{so}=10$ MeV fm^2 is the best choice. The depth of the nuclear interaction $V_N^{(0)}$ is adjusted so that the measured energy of a given state is reproduced.

The charge density of the core is parametrized in a similar fashion

$$\rho_D(r,\theta)=N_0 f\left(\frac{r-R_C\left[1+\sum_\lambda \beta_\lambda Y_{\lambda 0}(\theta)\right]}{a_C}\right). \tag{A4}$$

The volume integral of this density is normalized to one. The radius R_C is defined according to Eq. (A2) with $r_0=1.22$ fm, and we choose $a_C=0.56$ fm.

The Coulomb interaction of a proton with the core is

$$V_C(r,\theta)=\int d\mathbf{r}'\,\rho_D(r',\theta')\,\frac{Z_D e^2}{|\mathbf{r}-\mathbf{r}'|}.$$

Inserting into this expression the multipole expansion $\rho_D=\Sigma_\lambda \rho_\lambda(r)P_\lambda[\cos(\theta)]$ of the density, and also the multipole expansion of the point-Coulomb interaction, we obtain

$$V_C(r,\theta)=\sum_\lambda \frac{4\pi Z_D e^2}{2\lambda+1}P_\lambda[\cos(\theta)]\int_o^\infty dr'\,r'^2\frac{r_<^\lambda}{r_>^{\lambda+1}}\rho_\lambda(r'), \tag{A5}$$

where $r_<=\min(r,r')$ and $r_>=\max(r,r')$.

Let us point out that the parametrization of the deformed nuclear interaction (A1) assumes that the diffuseness is constant in the radial direction. The interactions discussed in Ref. [20], which have been applied to deformed proton emitters in Refs. [6–10], are calculated as functions of the minimum distance between the proton and the surface of the core. One can estimate the significance of this difference by replacing the distance $r-R(\theta)$ with its projection $[r-R(\theta)]\hat{r}\cdot\hat{n}$ onto a unit vector $\hat{n}$, which is perpendicular to surface of the core nucleus. If we choose the unit vector $\hat{n}$ at the intersection of $\mathbf{r}$ with the surface of the core we obtain $\hat{r}\cdot\hat{n}=R(\theta)/\sqrt{R^2(\theta)+[dR(\theta)/d\theta]^2}$. Inserting the projected distance into the expression for the nuclear interaction, Eq. (A1), we see that this correction is equivalent to using the angle-dependent diffuseness

$$a_{\rm eff}(\theta)=a\sqrt{1+\left(\frac{1}{R(\theta)}\frac{dR(\theta)}{d\theta}\right)^2}. \tag{A6}$$

This expression is consistent with Eq. (4-188c) of Ref. [12] to lowest order. We include this correction consistently (except otherwise stated) in all the expressions that make use of the deformed Fermi function, i.e., the nuclear and the spin-orbit interactions, and also the charge density of the core.

APPENDIX B: RESONANCE SOLUTIONS

Here we discuss how one can determine the resonance energy and wave function of a proton emitter. The coupled equations have the following general form:

$$(h_n-E)u_n(r)=-\sum_{n'} V_{nn'}(r)u_{n'}(r), \tag{B1}$$

where $n=(ljR)$, $h_n=h_{lj}+E_R$, and $V_{nn'}(r)$ represents the coupling matrix on the right side of Eq. (4). Assume that the total number of coupled equations is N. We can then generate N different sets of solutions by choosing N different sets of initial conditions at $r=0$. Let us denote these solutions by $\phi_{nn_0}(r)$, where n refers to the channels and n_0 refers to a particular choice of initial conditions. All solutions must be regular at $r=0$, i.e., $\phi_{nn_0}(r=0)=0$. A simple way to generate a particular set of solutions is for fixed n_0 to require that

$$u_{nn_0}(r)\to\delta_{nn_0}r^{l+1}\quad\text{for } r\to 0, \tag{B2}$$

i.e., only the channel $n=n_0$ has a nonzero wave function near the origin.

The coupled equations are solved N times with the different initial conditions (B2). They are solved from $r=0$ out to a large distance r_m, which is outside the range of the couplings. At $r=r_m$, the solutions can be matched to Coulomb wave functions

$$u_{nn_0}(r)=A_{nn_0}F_l(k_Rr)+B_{nn_0}G_l(k_Rr), \tag{B3a}$$

$$u'_{nn_0}(r)=A_{nn_0}F'_l(k_Rr)+B_{nn_0}G'_l(k_Rr). \tag{B3b}$$

Here the prime denotes a radial derivative, and $\hbar k_R=\sqrt{2\mu|E-E_R|}$ is the asymptotic momentum. When $E<E_R$, the Coulomb wave functions are replaced by those associated with bound state problems; see Eq. (8b).

Using the Wronskian $F'_lG_l-F_lG'_l=k_R$ we obtain

$$A_{nn_0}=\frac{1}{k_R}[G_l(k_Rr)u'_{nn_0}(r)-G'_l(k_Rr)u_{nn_0}(r)], \tag{B4a}$$

$$B_{nn_0}=\frac{1}{k_R}[F'_l(k_Rr)u_{nn_0}(r)-F_l(k_Rr)u'_{nn_0}(r)]. \tag{B4b}$$

A general set of solutions to the coupled equations, $\phi_n(r)$, can be expressed as

$$\phi_n(r)=\sum_{n_0}\alpha_{n_0}u_{nn_0}(r). \tag{B5}$$

For a spherical proton emitter, where there is only one channel, one can determine a resonance energy and wave function by requiring that the radial wave function is matched to the irregular Coulomb wave function $G_l(kr)$ outside the range of the nuclear field. This is done by varying the energy E until the A amplitude in Eqs. (B3a)–(B4) vanishes.

In the deformed case, we determine the resonance energy by requiring that the radial wave functions $\phi_{ljR}(r)$ match the associated Coulomb wave functions $G_l(k_Rr)$ at $r=r_m$. Inserting the asymptotic form Eq. (B3a) into Eq. (B5),

$$\phi_n(r)=\left(\sum_{n_0}\alpha_{n_0}A_{nn_0}\right)F_l(k_Rr)+\left(\sum_{n_0}\alpha_{n_0}B_{nn_0}\right)G_l(k_Rr), \tag{B6}$$

we see that we can make the regular solution $F_l(k_Rr)$ disappear if we can find a set of amplitudes α_{n_0} so that

$$\sum_{n_0}A_{nn_0}\alpha_{n_0}=0. \tag{B7}$$

This is possible if the determinant of the $N\times N$ matrix A_{nn_0} vanishes,

$$\det\{A_{nn_0}\}=0. \tag{B8}$$

This condition determines the resonance energy, and it is solved by a numerical search.

Once a resonance solution has been determined, it is normalized

$$\sum_n \int_0^{r_{\rm norm}} dr|\phi_n(r)|^2=1. \tag{B9}$$

The point is that the wave function of a proton resonance falls off dramatically as it passes through the Coulomb barrier, typically by 10 orders of magnitude [13]. A reasonable choice is $r_{\rm norm}=100$ fm, which is close to the outer classical turning point. After the solution has been normalized, one can then extract the amplitudes

$$N_{ljR}=\frac{\phi_{ljR}(r)}{G_l(k_R r)}, \quad \text{at } r=r_m, \tag{B10}$$

which determine the partial decay widths according to Eq. (7).

APPENDIX C: DEFORMED SPIN-ORBIT INTERACTION

The deformed spin-orbit interaction is expressed in the so-called Thomas form [19]

$$V_{ls}(r,\theta')=4V_{so}([\nabla f(r,\theta)]\times\mathbf{p})\cdot\mathbf{s}, \tag{C1}$$

where $f(r,\theta)$ is the deformed Fermi function used in Eq. (A1). Note that we use the convention $\hbar=1$ so that the dimension of V_{so} is MeV fm^2. Let us determine this interaction in spherical coordinates in the intrinsic system, with the z axis along the symmetry axis of the rotor. The necessary tools can be found in Chap. 9 of Ref. [26]. Thus the general expression for the gradient is

$$\nabla=\hat{r}\frac{d}{dr}+\hat{\theta}\frac{1}{r}\frac{d}{d\theta}+\hat{\phi}\frac{1}{r\sin(\theta)}\frac{d}{d\phi}, \tag{C2}$$

where $\hat{r}$, $\hat{\theta}$, and $\hat{\phi}$ are the unit vectors associated with the spherical coordinates.

Inserting Eq. (C2) into Eq. (C1) we obtain two terms. The first term is caused by the force in the radial direction

$$V_{ls}^{(1)}(r,\theta)=4V_{so}\frac{1}{r}\frac{df}{dr}(\mathbf{r}\times\mathbf{p})\cdot\mathbf{s}$$
$$=4V_{so}\frac{1}{r}\frac{df}{dr}\mathbf{l}\cdot\mathbf{s}. \tag{C3}$$

This part of the interaction can easily be included in the coupled equations.

The second part of the interaction, which is caused by the force in the θ direction, is more complicated to deal with,

$$V_{ls}^{(2)}(r,\theta)=4V_{so}\frac{1}{r}\frac{df}{d\theta}(\hat{\theta}\times\mathbf{p})\cdot\mathbf{s}. \tag{C4}$$

The force in the ϕ direction vanishes because of the assumed axial symmetry. Sherif demonstrated that the interaction (C4) plays an important role in reproducing the asymmetry of inelastic proton scattering at forward angles [19]. To evaluate this term we express the momentum operator $\mathbf{p}=-i\nabla$ in spherical coordinates as in Eq. (C2) and obtain

$$(\hat{\theta}\times\mathbf{p})\cdot\mathbf{s}=-i(\hat{\theta}\times\hat{r})\cdot\mathbf{s}\frac{d}{dr}+\frac{-i}{r\sin(\theta)}(\hat{\theta}\times\hat{\phi})\cdot\mathbf{s}\frac{d}{d\phi}$$
$$=i\hat{\phi}\cdot\mathbf{s}\frac{d}{dr}+\frac{1}{r\sin(\theta)}\hat{r}\cdot\mathbf{s}l_z. \tag{C5}$$

Let us now introduce the multipole expansion

$$f(r,\theta)=\sum_\lambda f_\lambda(r)P_\lambda[\cos(\theta)]. \tag{C6}$$

The first part of Eq. (C5) leads to a term of the form

$$\frac{dP_\lambda}{d\theta}i\hat{\phi}\cdot\mathbf{s}=-\frac{1}{2}\frac{dP_\lambda}{d\theta}(e^{i\phi}s_- - e^{-i\phi}s_+)$$
$$=-\frac{1}{2}([l_+,P_\lambda]s_- +[l_-,P_\lambda]s_+)$$
$$=-[\mathbf{l}\cdot\mathbf{s},P_\lambda], \tag{C7}$$

where we have used the commutator relation $[l_\pm,P_\lambda]=\pm e^{\pm i\phi}(dP_\lambda/d\theta)$. This term produces the interaction

$$V_{ls}^{(2a)}(r,\theta)=-4V_{so}\sum_\lambda\frac{f_\lambda}{r}[\mathbf{l}\cdot\mathbf{s},P_\lambda]\frac{d}{dr}. \tag{C8a}$$

The second part of Eq. (C5) contains the helicity operator $\hat{r}\cdot\mathbf{s}$ and results in the interaction

$$V_{ls}^{(2b)}(r,\theta)=-4V_{so}\sum_\lambda\frac{f_\lambda(r)}{r^2}\frac{dP_\lambda}{d\cos(\theta)}\hat{r}\cdot\mathbf{s}l_z. \tag{C8b}$$

We note that the three components of the spin-orbit interaction $V_{ls}^{(1)}$, $V_{ls}^{(2a)}$, and $V_{ls}^{(2b)}$, are not separately Hermitian but their sum is.

Matrix elements. In practical calculations we need the spin-angular matrix elements of the three interactions, Eqs. (C3),(C8a),(C8b), in the intrinsic system of the rotor. Fortunately, it turns out that the matrix elements are diagonal in K. Let us introduce the abbreviated notation: $N=ljK$ of the spin-angular states. Then Eq. (C3) produces the coupling

$$\langle N_1|V_{ls}^{(1)}|N_2\rangle=2V_{so}[j_2(j_2+1)-l_2(l_2+1)-3/4]$$
$$\times\sum_\lambda\langle N_1|P_\lambda|N_2\rangle\frac{1}{r}\frac{df_\lambda}{dr}, \tag{C9}$$

where the matrix element $\langle N_1|P_\lambda|N_2\rangle$ is given in Eq. (20).

The coupling which is generated by Eq. (C8a) is

$$\langle N_1|V_{ls}^{(2a)}|N_2\rangle = 2V_{so}(j_2(j_2+1)-l_2(l_2+1)-j_1(j_1+1) + l_1(l_1+1))\sum_\lambda \langle N_1|P_\lambda|N_2\rangle \frac{f_\lambda}{r}\left(\frac{d}{dr}-\frac{1}{r}\right). \tag{C10}$$

This coupling acts on the radial wave functions $\phi_{lj}(r)$. The operator d/dr in Eq. (C8a) has therefore been replaced by $(d/dr-1/r)$ in Eq. (C10).

To calculate matrix elements of Eq. (C8b) we insert intermediate states $N'=l'j'K'$,

$$\langle N_1|V_{ls}^{(2b)}|N_2\rangle = -4V_{so}\sum_\lambda \frac{f_\lambda}{r^2}\sum_{N'} \langle N_1|\frac{dP_\lambda}{d\cos(\theta)}\hat{r}\cdot\mathbf{s} \times|N'\rangle\langle N'|l_z|N_2\rangle. \tag{C11}$$

The matrix element of l_z is diagonal in K and l (i.e., $l'=l_2$ and $K'=K$) but not in j,

$$\langle N'|l_z|N_2\rangle = \sum_{m_l m_s} m_l\langle l_2 m_l \tfrac{1}{2} m_s|j'K\rangle\langle l_2 m_l \tfrac{1}{2} m_s|j_2K\rangle.$$

To calculate the first matrix element in Eq. (C11) we insert

$$\frac{dP_\lambda(z)}{dz} = \sum_{\lambda'=1}^{\lambda-1}(2\lambda'+1)P_{\lambda'}(z),$$

where the sum is over odd values of λ', assuming that λ is even. The first matrix element in Eq. (C11) can now be calculated in the helicity representation; see Eq. (3A-5) of Ref. [16]. The final expression is

$$\langle N_1|\frac{dP_\lambda}{d\cos(\theta)}\hat{r}\cdot\mathbf{s}|N'\rangle = \sum_{\lambda'=1}^{\lambda-1}\frac{2\lambda'+1}{2}\langle j'K\lambda'0|j_1K\rangle \times\langle j_1\tfrac{1}{2}\lambda'0|j'\tfrac{1}{2}\rangle,$$

where the sum is over odd values of λ', whereas λ and l_1+l_2 are even numbers.

[1] C. N. Davids *et al.*, Phys. Rev. Lett. **80**, 1849 (1998).
[2] A. A. Sonzogni *et al.*, Phys. Rev. Lett. **83**, 1116 (1999).
[3] K. Rykaczewski *et al.*, Phys. Rev. C **60**, 011301(R) (1999).
[4] P. Möller, J. R. Nix, W. D. Myers, and W. J. Swiatecki, At. Data Nucl. Data Tables **59**, 185 (1995).
[5] V. P. Bugrov and S. G. Kadmensky, Sov. J. Nucl. Phys. **49**, 967 (1989); Phys. At. Nucl **59**, 424 (1996).
[6] L. S. Ferreira, E. Maglione, and R. J. Liotta, Phys. Rev. Lett. **78**, 1640 (1997).
[7] E. Maglione, L. S. Ferreira, and R. J. Liotta, Phys. Rev. Lett. **81**, 538 (1998).
[8] E. Maglione, L. S. Ferreira, and R. J. Liotta, Phys. Rev. C **59**, R589 (1999).
[9] E. Maglione and L. S. Ferreira, Phys. Rev. C **61**, 047307 (2000).
[10] A. T. Kruppa, B. Barmore, W. Nazarewicz, and T. Vertse, Phys. Rev. Lett. **84**, 4549 (2000).
[11] C. N. Davids and H. Esbensen, Phys. Rev. C **61**, 054302 (2000).
[12] A. Bohr and B. R. Mottelson, *Nuclear Structure* (Benjamin, Reading, MA, 1975), Vol. II.
[13] S. Åberg, P. B. Semmes, and W. Nazarewicz, Phys. Rev. C **56**, 1762 (1997); **58**, 3011 (1998).
[14] N. K. Glendenning, *Direct Nuclear Reactions* (Academic, New York, 1983).
[15] M. Gell-Mann and M. L. Goldberger, Phys. Rev. **91**, 398 (1953).
[16] A. Bohr and B. R. Mottelson, *Nuclear Structure* (Benjamin, New York, 1969), Vol. I.
[17] A. K. Kerman, Mat. Fys. Medd. K. Dan. Vidensk. Selsk. **30** (1956).
[18] A. Henriquez, T. Engeland, and J. Rekstad, Phys. Rev. C **27**, 1302 (1983).
[19] H. Sherif, Nucl. Phys. **A131**, 532 (1969).
[20] S. Cwiok, J. Dudek, W. Nazarewicz, J. Skalski, and T. Werner, Comput. Phys. Commun. **46**, 739 (1987).
[21] R. R. Chasman, Phys. Lett. B **187**, 219 (1987).
[22] V. Zamfir (private communication).
[23] D. Seweryniak (private communication).
[24] F. D. Becchetti and G. W. Greenlees, Phys. Rev. **182**, 1190 (1969).
[25] L. Rosen, J. G. Beery, and A. S. Goldhaber, Ann. Phys. (N.Y.) **34**, 96 (1965).
[26] E. Merzbacher, *Quantum Mechanics*, 2nd ed. (Wiley, New York, 1970).